Re-evaluating metamorphism in the southern Natal Province, South Africa

Eleanore Blereau[1,2]* and Christopher Spencer[1,3]

[1]School of Earth and Planetary Sciences, Institute for Geoscience Research (TIGeR), Curtin University, GPO Box U1987, Perth, WA 6845, Australia

[2]John de Laeter Centre, Curtin University, GPO Box U1987, Perth, WA 6845, Australia

[3]Department of Geological Sciences and Geological Engineering, Queen's University, Kingston, Ontario, Canada K7L 3N6

EB, 0000-0001-8850-397X; CS, 0000-0003-4264-3701

Present addresses: EB, School of Earth and Environment, University of Leeds, Leeds LS2 9JT, UK

*Correspondence: earebl@leeds.ac.uk

Abstract: The metamorphic conditions of the Natal Metamorphic Province (NMP) have been the focus of previous studies to assist with Rodinia reconstructions but there are limited constraints on the age of metamorphism. We use a combination of modern techniques to provide new constraints on the conditions and timing of metamorphism in the two southernmost terranes: the Mzumbe and Margate. Metamorphism reached granulite facies, 780–834°C at 3.9–7.8 kbar in the Mzumbe Terrane and 850–892°C at 5.7–6.1 kbar in the Margate Terrane. The new pressure and temperature constraints are supportive of isobaric cooling in the Margate Terrane as previously proposed. Peak metamorphism of the two terranes is shown to have occurred *c.* 40 myr apart, which contrasts strongly with previous assumptions of coeval metamorphism. While the age of peak metamorphism of the Margate Terrane (1032.7 $\pm$ 4.7 Ma) coincides with the tectonism and magmatism associated with the emplacement of the Oribi Gorge Suite (*c.* 1050–1030 Ma), the age of metamorphism of the Mzumbe Terrane (987.4 $\pm$ 8.1 Ma) occurs *c.* 30–40 myr after tectonism is previously thought to have finished. We propose that models of advective cooling during transcurrent shearing can explain the metamorphic conditions and timing of the NMP.

Supplementary material: T–XH2O diagrams used for the generation of final P–T pseudosections and complete monazite U-Pb geochronology and garnet REE datasets are available at https://doi.org/10.6084/m9.figshare.c.6488823

Metamorphic terranes, in particular high-grade terranes, present a complex challenge when constraining and differentiating between interconnected geological processes (e.g. partial melting and fluid flux: Taylor *et al.* 2014; Blereau *et al.* 2016; Carvalho *et al.* 2019; Wang *et al.* 2021) and overprinting from subsequent events (e.g. polymetamorphism: Blereau *et al.* 2017, 2019; Laurent *et al.* 2018*a*, *b*). This amalgamation of processes and events often makes it difficult to determine clearly the duration and conditions of discrete metamorphic episodes (i.e. a discrete pressure–temperature–time (*P–T–t*) path). The petrochronological approach (Kylander-Clark *et al.* 2013; Kohn 2016; Engi *et al.* 2017), a multidisciplinary investigation of processes that connect major silicate mineral evolutions (petrology and *P–T* constraints) to a range of analytical data from major and accessory minerals (e.g. geochemistry and geochronology), has been applied to an array of geological systems. Petrochronology has allowed us to refine our understanding metamorphic processes (e.g. REE systematics in zircon during high-grade metamorphism: Whitehouse 2003; Holder *et al.* 2015; Taylor *et al.* 2016; Rubatto 2017; Taylor *et al.* 2017; Blereau *et al.* 2022) and constrain *P–T–t* paths for short (e.g. Viete and Lister 2017) and prolonged metamorphic events (e.g. Clark *et al.* 2018). Petrochronology is a powerful field of research as all data used in this approach require the retainment of the broader geological context on the microscopic level and potentially up to the field level.

The Mzumbe and Margate terranes of the Natal Metamorphic Province (NMP) have historically been interpreted to have been metamorphosed together during the emplacement of the Oribi Gorge Suite in an early stage of metamorphism

From: van Schijndel, V., Cutts, K., Pereira, I., Guitreau, M., Volante, S. and Tedeschi, M. (eds) 2024. *Minor Minerals, Major Implications: Using Key Mineral Phases to Unravel the Formation and Evolution of Earth's Crust*. Geological Society, London, Special Publications, **537**, 313–331.
First published online May 18, 2023, https://doi.org/10.1144/SP537-2022-222

(M_1) (McCourt *et al.* 2006; Eglington *et al.* 2010; Grantham *et al.* 2012); however, metamorphism in this area is poorly dated (the only direct metamorphic ages are from Spencer *et al.* 2015) and needs the development of a metamorphic and deformational geochronological framework. This geochronology has additional importance as this region provides information on the early history of Rodinia, as the NMP comprises several terranes that accreted onto the Kaapvaal Craton in the late Mesoproterozoic during to the assembly of Rodinia (Jacobs and Thomas 1994). We revisit the metamorphic evolution of the NMP in order to better understand the relationship between the Mzumbe and Margate terranes during metamorphism, and the re-evaluate the peak metamorphic conditions experienced.

Regional geology

The NMP is part of the Rodinia-age (*c.* 1.1 Ga) Namaqua–Natal Belt and is subdivided into three terranes: the Tugela Terrane, the Mzumbe Terrane and

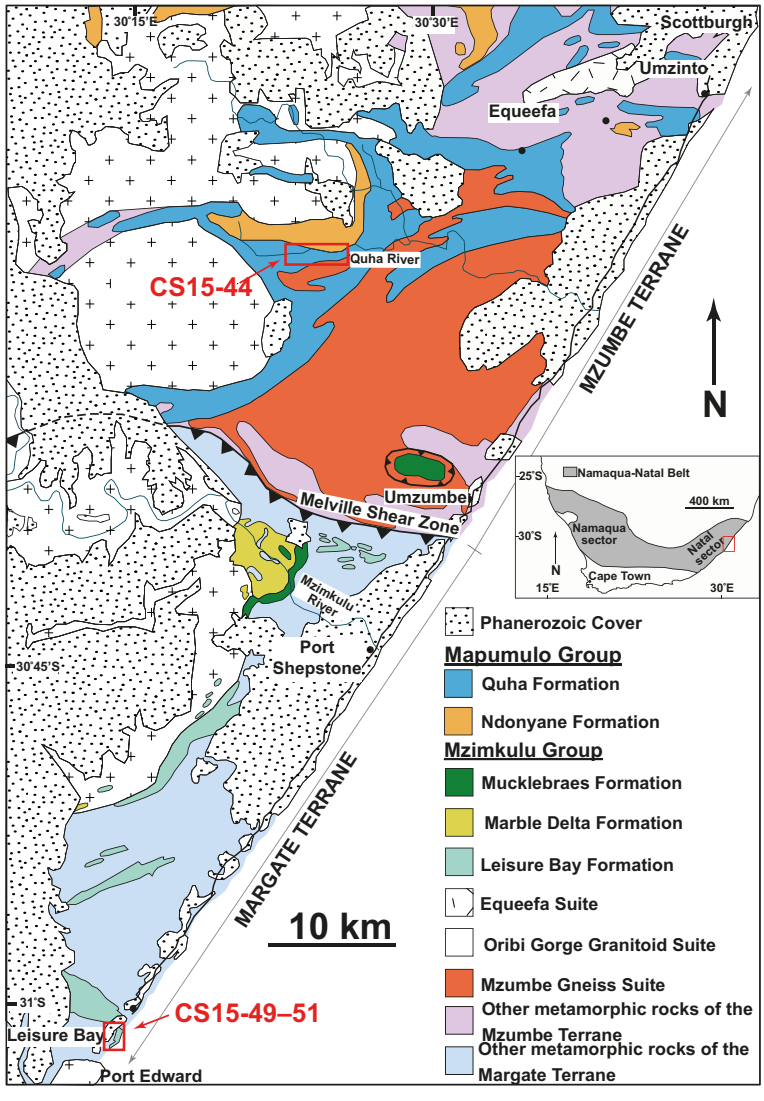

Fig. 1. Simplified geological map of the Margate and Mzumbe terranes within the Natal Metamorphic Province showing the locations of samples analysed in this study. Modified after Thomas (1990), Grantham *et al.* (1991), Thomas *et al.* (1991*a*, *b*) and Thomas (1992*a*, *b*). Inset map of the Namaqua–Natal Belt showing the location of the field area, modified after Spencer *et al.* (2015).

Table 1. *Summary of existing constraints on the metamorphic evolution of the Mzumbe and Margate terranes*

Temperature (T) (°C)	Pressure (P) (kbar)	Metamorphic event	Method	Reference
Mzumbe Terrane				
No constraints	No constraints	Earlier event?	Not applicable	Evans (1984); Evans *et al.* (1987)
750–800	6–8	Dominant event	Compilation of experimental stabilities of different mineral assemblages	Evans *et al.* (1987)
c. 650	*c.* 6	Retrograde event	Epidote growth	Evans *et al.* (1987)
850/1100		Dominant event	Two pyroxene thermometry for Cpx and Ca-rich Cpx, respectively	Thomas *et al.* (1992*b*)
	5–8	Dominant event	Geobarometry	Grantham (1983); Evans *et al.* (1987); Thomas *et al.* (1992*a*)*
830–1030		Dominant event	Thermo-Calc (version from Powell and Holland 1988)	Grantham *et al.* (1993)
Margate Terrane				
434–1110		Dominant event	Garnet pair thermometer	Mendonidis and Grantham (2003)
>850	*c.* 4	Dominant event	Mineral stability in P–T grids and Thermo-Calc version 2.7	Mendonidis and Grantham (2003)
c. 800	7.5–9	Secondary event	GAES barometer	Mendonidis and Grantham (2003)

*Pressure conditions, except for those in Evans *et al.* (1987), are all from samples from the neighbouring Margate Terrane, not from the Mzumbe Terrane, but are used in the Mzumbe Terrane.

the Margate Terrane (Thomas 1989). This study focuses on metamorphic rocks within the Mzumbe and Margate terranes, which are separated by the Melville Shear Zone (Fig. 1). The metamorphic history of the Mzumbe and Margate terranes (Table 1) is historically assumed to have occurred coevally at *c.* 1090–1040 Ma, despite there being no direct metamorphic ages available for the Mzumbe, and to be similar in tectonic style (Eglington *et al.* 2003; Mendonidis *et al.* 2015; Spencer *et al.* 2015). Previous attempts to establish ages of metamorphism were achieved through dating cross-cutting igneous rocks. The Mzumbe and Margate terranes (along with the Tugela Terrane north of the Mzumbe Terrane) were assembled during a multistage accretion event during the Natal Orogeny (Spencer *et al.* 2015; Mendonidis and Thomas 2019). The Mzumbe Terrane is interpreted to record protracted oceanic arc magmatism from *c.* 1200–1160 Ma (represented by the Mzumbe plutonic suite) followed by accretion onto the southern margin of the Kaapvaal Craton at *c.* 1150 Ma (Spencer *et al.* 2015 and references therein). The Margate Terrane largely records a similar magmatic history but has been interpreted to represent a separate, coeval, oceanic arc (Mendonidis *et al.* 2015). Following accretion and metamorphism, transcurrent deformation and syn- to post-orogenic plutons (Oribi and Sezela plutonic suites) are proposed to have dominated the region from *c.* 1080 to *c.* 1030 Ma (Eglington *et al.* 2003; Mendonidis *et al.* 2015; Spencer *et al.* 2015). In the following subsections we summarize the existing constraints on each terrane from the original literature, as more recent literature often misquotes these constraints.

Mzumbe Terrane

The Mzumbe Terrane comprises the intermediate-mafic and psammitic Quha Formation, acid Ndonyane Formation (both part of the Mapumulo Group), and a number of magmatic suites including the Equeefa Suite, the intensely deformed Mzumbe Gneiss Suite (or Mzumbe Granitoid Suite) and a suite of S-type granites (Thomas *et al.* 1991*a*; Thomas 1992*a*). The Quha Formation is the oldest supracrustal gneiss sequence in the Mzumbe Terrane with a minimum formation age of *c.* 1235 Ma (Thomas and Eglington 1990; Thomas *et al.* 1999), and is a layered sequence of semi-pelitic, pelitic, calc-silicate and magnesian gneisses, with minor amounts of marble and amphibolite. The Mzumbe Terrane is interpreted to have a polymetamorphic history with an earlier episode that has no constrained P–T

conditions (M_1) and a more dominant metamorphic event (M_2). M_1 is represented by small quartzofeldspathic veins intruding the Quha Formation (i.e. Banded Gneiss Formation in Evans *et al.* 1987) and pre-M_2 garnets, with an assemblage of biotite, hornblende, cordierite and fibrolite tentatively interpreted as the assemblage of this event (Evans 1984; Evans *et al.* 1987). Evans *et al.* (1987) compiled *P–T* constraints on the dominant metamorphic event (M_2) based on a number of lithological assemblages around the Umizinto region (north in Fig. 1). The synthesis of the experimental stabilities for different mineral assemblage and reactions yielded granulite-facies conditions of 750–800°C at 6–8 kbar (Evans *et al.* 1987). Following peak-M_2 metamorphism, cooling caused the development of Fe-rich epidote, with *P–T* conditions estimated to have been below *c.* 6 kbar and 650°C.

Also within the Mzumbe Terrane, the mafic Equeefa Suite was used in an attempt to constrain M_2 metamorphism. Two-pyroxene thermometry (after Lindsley 1983) yielded magmatic conditions of *c.* 1100°C from clinopyroxene and an interpreted metamorphic temperature of *c.* 850°C from more calcic clinopyroxene (Thomas *et al.* 1992*b*). Using an early version of the Thermo-Calc software (Powell and Holland 1988), Grantham *et al.* (1993) modelled reaction curves relating to two corona reactions (between olivine–plagioclase and phlogopite–plagioclase) and the reaction between olivine and phlogopite within the olivine melanorite within the Equeefa Suite. The pressure conditions used in the aforementioned phase equilibria models were based on previous geobarometry estimates by Grantham (1983), Evans *et al.* (1987) and Thomas *et al.* (1992*a*) (5–8 kbar). Although, aside from Evans *et al.* (1987), the pressure constraints used within Grantham (1983) and Thomas *et al.* (1992*a*) are all from granulite-facies rocks within the neighbouring Margate Terrane not from the Mzumbe Terrane. The stability of the Ol–Pl corona reaction in the olivine melanorite (olivine next to plagioclase is overgrown by orthopyroxene then clinoamphibole) was shown to be affected by water activity (a_{H_2O}), with a change in a_{H_2O} from 1.0 to 0.1 reducing the reaction temperature from *c.* 1030 to 830°C at 7 kbar. The Phl–Pl coronas (pargasite at the Phl–Pl interface) were difficult to model due to extensive solid solutions in all phases, making it difficult to define end members as a result of the applied models containing no solid solutions. Solid solutions were not introduced into Thermo-Calc until 1990 (Guiraud *et al.* 1990) and activity compositions appropriate for modelling melt-bearing mafic compositions only became available in 2016 (Green *et al.* 2016). The Ol–Phl reaction was also shown to be sensitive to a_{H_2O} but had to assume the presence of earlier K-feldspar, although no K-feldspar remains within the olivine melanorite.

Margate Terrane

The Margate Terrane contains three main formations: the Leisure Bay, Marble Delta and Mucklebraes formations, which form the Mzimkulu Group. Similar to the Quha Formation, the Leisure Bay Formation is the oldest supracrustal gneiss sequence within the Margate Terrane, and is a layered sequence of pelitic, semi-pelitic and calcic paragneisses, with minor kinzigite and metabasic gneisses (Thomas *et al.* 1991*c*; Thomas 1992*b*). *P–T* estimates for this region are based on a number of garnet mineral pair thermometers (i.e. Grt–Bt, Grt–Opx, Grt–Crd and Grt–Ilm), yielding a wide range of possible temperatures from as low as *c.* 434°C to as high as *c.* 1110°C, which is likely to be due to re-equilibration upon cooling (Mendonidis and Grantham 2003). Using experimental *P–T* grids and an early versions of the Thermo-Calc software (version 2.7, *c.* 1998), *P–T* estimates for M_1 based on the stability of spinel, cordierite and hypersthene yielded temperatures >850°C and pressures of *c.* 4 kbar, followed by isobaric cooling (Mendonidis and Grantham 2003). The Leisure Bay rocks utilized by Mendonidis and Grantham (2003) are intercalated with the Munster Suite that intruded at *c.* 1090 Ma, which was interpreted to have resulted in M_1, but the Leisure Bay rocks have not been directly dated. M_2 was restricted to fertile rocks and is less evident in the Leisure Bay rocks due to previous partial melting during M_1, with the breakdown of biotite in fertile lithologies leading to garnet growth and partial melt formation (Mendonidis and Grantham 2003). M_2 occurred at a higher pressure (7.5–9 kbar: GAES barometer) in order for only garnet to form from incongruent melting instead of garnet + cordierite + hypersthene as seen in M_1, with anatexis occurring at *c.* 800°C (Mendonidis and Grantham 2003). M_1 metamorphism in the Margate Terrane and M_2 in the Mzumbe Terrane are both interpreted to follow *P–T* paths with limited pressure variations (Grantham *et al.* 1994; Mendonidis and Grantham 2003). The *P–T* path for M_2 in the Margate Terrane is interpreted to be clockwise but at higher pressure (Mendonidis and Grantham 2003). There is a lot of variability within these pre-existing constraints and, with the lack of a firm geochronological framework for the metamorphic history of this region, a re-examination and collection of *in situ* data and more modern techniques could clarify existing data.

Thanks to updated activity models we now have the opportunity to refine and re-evaluate the existing *P–T* constraints to determine whether the style and conditions between the Margate and Mzumbe terranes are truly similar. Using monazite U–Pb geochronology we investigated the age of peak metamorphism to provide some much-needed new data. The samples collected for this study will

not only aid in evaluating the metamorphic conditions and timing but will further refine the tectonic history between the Mzumbe Terrane and the Margate Terrane.

Methods

Electron microprobe analyser

Electron microprobe analyses and X-ray compositional maps were made using a Cameca SX-50 electron microprobe at the Department of Geological Sciences, Brigham Young University, Utah, USA. Backscatter electron images and element maps of Fe, Mg, Ca, Mn were made of the phases selected for probe analyses. X-ray maps were used to determine appropriate locations for analyses, and were collected with an acceleration voltage of 15 kV, a current of 40 nA and a time per pixel of 20 ms. Point analyses and/or transects were conducted across garnet, biotite, muscovite and plagioclase to further characterize the compositional zoning and to find appropriate areas for thermobarometric calculations. The analytical conditions used for quantitative analyses of silicates were 15 kV acceleration voltage, 20 s count time and 10–20 nA current. Natural minerals were used as standards to calibrate the compositions of unknown minerals.

Laser ablation inductively coupled plasma mass spectrometer (LA-ICP-MS)

Garnet trace element analyses. Rare earth element (REE) and other trace element compositions of garnet were measured by LA-ICP-MS using an ASI RESOlution M-50A-LR laser ablation system, using a Compex 193 nm Ar-F excimer laser and an Agilent 7700 inductively coupled plasma mass spectrometer at Curtin University. Garnet was analysed in polished thin sections using a 50 µm spot size and 30 s analyses at a repetition rate of 7 Hz. NIST glass 610 (Pearce *et al.* 1997) was used as the primary trace element reference materials, with NIST 612 as the secondary standard. Stoichiometric Si (18 wt%) was assumed for calibration of garnet trace elements. Time-resolved data were processed using Iolite software (version 3.1: Paton *et al.* 2010, 2011). Trace elements were normalized relative to chondrite based on the values of Anders and Grevesse (1989).

Monazite U–Pb geochronology. Individual monazite grains (mounted and polished in 1 inch epoxy rounds) were ablated using a Resonetics RESOlution M-50A-LR laser ablation system, incorporating a Compex 102 excimer laser. Following a 15–20 s period of background analysis, samples were spot ablated for 30 s at a 7 Hz repetition rate using a 23 µm beam and laser energy of 1.7 J cm^{-2} at the sample surface. The sample cell was flushed by ultra-high purity He (0.68 l min^{-1}) and N_2 (2.8 ml min^{-1}). Isotopic intensities were measured using an Agilent 7700s quadrupole ICP-MS with high-purity Ar as the plasma gas (flow rate 0.98 l min^{-1}). The dwell time for ^{204}Pb, ^{206}Pb, ^{207}Pb and ^{208}Pb was 0.03 s, and 0.0125 s for ^{232}Th and ^{238}U.

The primary reference material used for U–Pb dating in this study was 44069 ($^{206}Pb/^{238}U$ age 424.9 ± 0.4 Ma: Aleinikoff *et al.* 2006), with Moacyr ($^{206}Pb/^{238}U$ age 515.7 ± 0.7 Ma: Horstwood *et al.* 2016), Stern ($^{206}Pb/^{238}U$ age 512.4 ± 0.3 Ma: Horstwood *et al.* 2016) and Trebilcock ($^{206}Pb/^{238}U$ age 272 ± 2 Ma: Tomascak *et al.* 1996) used as secondary age reference materials. During the analytical session, 44069 yielded a $^{206}Pb/^{238}U$ weighted average age of 423.5 ± 2.7 Ma (MSWD = 0.6, $n = 18$; self-normalized). Moacyr yielded a $^{206}Pb/^{238}U$ weighted average age of 508.1 ± 4.6 Ma (MSWD = 1.7, $n = 9$), Stern a $^{206}Pb/^{238}U$ weighted average age of 503.7 ± 3.0 Ma (MSWD = 0.3, $n = 18$) and Trebilcock a $^{206}Pb/^{238}U$ weighted average age of 270.6 ± 1.9 Ma (MSWD = 0.3, $n = 13$). $^{206}Pb/^{238}U$ ages calculated for the secondary reference materials, treated as unknowns, were found to be within 2% of the accepted value and therefore no addition of excess variance to the systematic uncertainty was warranted. The time-resolved mass spectra were reduced using the U_Pb_Geochronology3 data reduction scheme in Iolite version 3.1 (Paton *et al.* 2011 and references therein). U–Pb data (including weighted mean and MSWD interpretation) were evaluated using the methodology of Spencer *et al.* (2016) and plotted using a Java-based computer application, KD*X* (Spencer *et al.* 2017).

Phase equilibrium modelling

Metamorphic *P–T* conditions were constrained using pseudosections modelled in the Na_2O–CaO–K_2O–FeO–MgO–Al_2O_3–SiO_2–H_2O–TiO_2–O (NCKFMASHTO) system. Thermo-Calc version 3.40i and the internally consistent dataset of Holland and Powell (2011) (tc-ds62 generated on 6 February 2014) was used with the activity composition models from White *et al.* (2014*a*). Mn-bearing solution models are available (White *et al.* 2014*b*); however, the effect of Mn at high temperatures is negligible (Johnson *et al.* 2015) and was not considered for this study. Calculations considered the phases: garnet, silicate melt, plagioclase, K-feldspar, epidote, biotite, orthopyroxene, cordierite, spinel-magnetite, ilmenite, rutile, sillimanite, kyanite, quartz, muscovite, sphene and chlorite.

Bulk rock compositions of the metapelites were determined by X-ray fluorescence (XRF) analysis

on a Siemens SRS 303 X-ray fluorescence spectrometer at the Department of Geological Sciences at Brigham Young University, USA. The XRF bulk compositions are given in Figure 9. The material used for the bulk composition for CS15-44 contained visible garnet that was not able to be captured in thin section but was assumed to be part of the peak assemblage. The Thermo-Calc-normalized bulk compositions (expressed in mol% oxides) used in the creation of the *P–T* pseudosections are given in Figure 9. The ferric iron content was assumed to equal 20% of the ferrous iron for all samples, which replicated the observed assemblages and appropriate oxides. Modelled H_2O contents in the metapelites were constrained using *T–X* pseudosections ranging from a quantity assuming all analysed loss on ignition as H_2O (loss on ignition (LOI): $X = 0$) to lower values (0.1 mol% at $X = 1$). The H_2O content chosen for the *P–T* modelling of the metapelites was such that the solidus was close to the field containing the peak assemblage whilst also avoiding the stabilization of sillimanite, which is absent in all samples, to higher temperatures (see Supplementary material Figures S1–S4).

TESCAN Integrated Mineral Analysis

Mineral phase maps based on energy dispersive X-ray spectroscopy (EDX) and backscattered electron (BSE) responses were created using the TESCAN Integrated Mineral Analysis (TIMA) multidetector scanning electron microscope and Oxford Instrument Aztec software located at the John de Laeter Centre at Curtin University. These phase maps were used to quantify the modality of minerals as a direct output from the Aztec software and confirm the identity of all mineral phases.

Sample descriptions

Quha Formation of the Mzumbe Terrane

The single gneissic sample (CS15-44) from the Quha Formation was collected from Stratotype B from Thomas *et al.* (1991*b*) along the Mkomazi River (Figs 1 & 2a). The stratotype comprises semi-pelitic gneiss, pelitic gneiss, amphibolite, calc-silicate gneiss, marble, psammite and quartzite.

CS15-44 (−30.13440° S, 30.55254° E). CS15-44 is a quartzofeldspathic semi-pelitic gneiss (Figs 2b & 3). The sample is mainly composed of plagioclase (*c.* 34.5%), K-feldspar (*c.* 31%) and quartz (*c.* 31%) (Fig. 3), with rare inclusion-rich garnet porphyroblasts (Fig. 2b, inset) and minor ilmenite and magnetite. No garnets were present within our thin section but they were present within localized patches of incipient melt within the melanosome in outcrop (Fig. 2b). Biotite (*c.* 2.5%) is present in minor amounts with all matrix phases. Even smaller amounts of muscovite are interpreted as retrograde. Evidence of another unknown, likely mafic, mineral is seen in rare completely chloritized pseudomorphs. Minor myrmekite is also present near plagioclase. Monazite is located along the foliation bounded by quartz, plagioclase and K-feldspar.

Leisure Bay Formation of the Margate Terrane

The three metapelitic samples (CS15-49–CS15-51: Figs 4 & 5) from the Leisure Bay Formation were collected at Port Edward from the key outcrop between the Port Edward and Nicholson's Point granites (Figs 1 & 6a). This is the type locality for this formation. The samples fall in a transect between the two plutons, with sample CS15-49 being the closest and CS15-51 being the most distal to the Nicholson's Point granite, and the inverse in relation to the Port Edward granite. Sample CS15-49 is within *c.* 50 m of the contact of the Nicholson's Point granite and sample CS15-51 is within *c.* 1 m of the Port Edward granite. All samples show evidence of partial melting at the outcrop scale with centimetre-scale leucosomes (Fig. 6b). Thin sections were made predominantly from the melanosome of the migmatite with only small-scale leucosomes.

CS15-49 (−31.02408° S, 30.24483° E). CS15-49 is a pelitic gneiss with large anhedral garnet porphyroblasts (*c.* 0.5–2.5 cm; *c.* 31%) (Figs 4a & 5a, b). The porphyroblasts contain large sporadic inclusions of biotite and quartz, and smaller pyrrhotite inclusions. The matrix is largely composed of K-feldspar (*c.* 24%) followed by lesser amounts of cordierite (*c.* 18%), quartz (*c.* 13%), plagioclase (*c.* 7%), biotite (*c.* 5%), and trace amounts of ilmenite and pyrrhotite. Quartz fills embayments within the garnet. Cordierite is partly replaced by muscovite (sericite), and ilmenite is seen breaking down to an intergrowth of rutile, quartz and pyrrhotite. Monazite occurs within the matrix as well as at the margins of or within garnet. Trace amounts of apatite occur within the matrix.

CS15-50 (−31.02599° S, 30.24484° E). CS15-50 is a pelitic gneiss with two distinct compositional layers (Figs 4b & 5c–d). Anhedral–subhedral garnet porphyroblasts (*c.* 19%; 0.5–4 mm) are mainly found within K-feldspar-rich layers (*c.* 9%) but also as smaller grains in lesser amounts (0.5–1.5 mm) within plagioclase-rich layers (*c.* 46%). Garnet porphyroblasts preserve biotite, ilmenite, pyrrhotite and quartz inclusions across both layers. The garnet and K-feldspar-rich layers record a larger amount of late randomly orientated biotite (*c.* 10%) than the plagioclase-rich layers, with biotite abutting

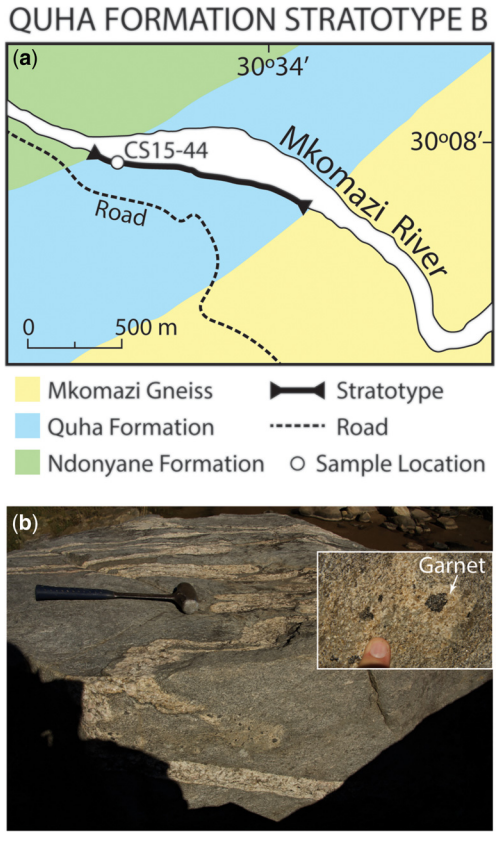

Fig. 2. (**a**) Simplified geological map of the Quha Formation stratotype B showing the sample locations. (**b**) Field photograph of the Quha quartzofeldspathic semi-pelitic gneiss with folded leucosomes. Rare garnet porphyroblasts rich in inclusions are visible, with a closer view shown in the inset. The geological hammer is for scale.

and growing around garnet porphyroblasts and with feldspar. The K-feldspar-rich layers also contain minor amounts of cordierite (*c.* 2%) and quartz (*c.* 5%). The plagioclase-rich layers contain a larger amount of quartz as well as orthopyroxene (*c.* 6%), which varies in grain size from similar sizes as the smaller garnet porphyroblasts to fine grained material (<0.5–2 mm). Quartz melt films can be seen at the edges of garnet and orthopyroxene within the plagioclase-rich layer, as well as rare intergrowths between biotite and quartz. Rare muscovite, trace pyrrhotite and ilmenite are seen in the matrix of both layers. Monazite occurs in the matrix, as well as grains at the margins of garnet or as inclusions. Trace amounts of apatite occur within the matrix.

CS15-51 (−31.02662° S, 30.24458° E). CS15-51 is also a pelitic gneiss and is the most homogeneous sample of the three collected from the Leisure Bay Formation (Figs 4c & 5e–f). Garnet porphyroblasts (*c.* 13%; <0.5–1 mm) are anhedral and embayed with large quartz inclusions, as well as with minor ilmenite and trace pyrrhotite inclusions. Some grains of garnet show fine wormy inclusions/intergrowth of quartz. Fine- to coarse-grained orthopyroxene (*c.* 3.5%) appears to have grown coevally with garnet, based on the lack of orthopyroxene inclusions and corona structures, and also shows irregular grain shapes such as for garnet. Similar to garnet, orthopyroxene has been disaggregated from *c.* 2 mm grains to grains that are 1 mm or smaller. The matrix is predominantly composed of quartz (*c.* 42%) and plagioclase (*c.* 34.5%), with minor K-feldspar (*c.* 1%), cordierite (*c.* 1.4%), ilmenite, muscovite and trace pyrrhotite. Biotite (*c.* 3%) appears as a late phase, reacting near orthopyroxene and garnet, crystallizing when H_2O is released as the partial melt crystallizes. Cordierite grains are rimmed by plagioclase, with garnet encapsulated or rimmed by quartz, both of which are likely to be melt films. Monazite occurs mainly in the matrix, with some grains at the margins of garnet. Trace amounts of apatite are present within the matrix.

Results

EPMA

Electron microprobe analysis of garnets from samples CS15-49–CS15-51 showed that garnets from all three Leisure Bay samples are consistently almandine-rich (*c.* 64–69 mol%), with lesser amounts of pyrope (*c.* 26–29 mol%) and minor grossular and spessartine contents (*c.* 2.5–3.5 and *c.* 1.5–2.5 mol%, respectively). X-ray maps of Fe, Ca, Mg and Mn show no major element geochemical zoning relating to core or rim textures in any of the three samples (i–iv in Fig. 7a–c).

Garnet trace elements

LA-ICP-MS analysis of garnets from all three Leisure Bay samples (CS15-49–CS15-51) targeted cores (inclusion rich) and rims (inclusion poor). Garnet cores from all three samples showed near flat mid-to-heavy REE (MREE–HREE) slopes (Yb/Gd slopes of *c.* 1–6) with normalized Lu (Lu_N) concentrations between 200 and 1000 chondrite normalized values (v in Fig. 7a–c). Garnet cores in sample CS15-51 had the least amount of scatter to the MREE–HREE with Yb/Gd slopes of 0.45–1.5. Garnet rims from all samples showed near flat to shallowly negative MREE–HREE slopes (0.45–2) with similar to slightly depleted HREE concentrations (Lu_N = 100–600) (v in Fig. 7a–c).

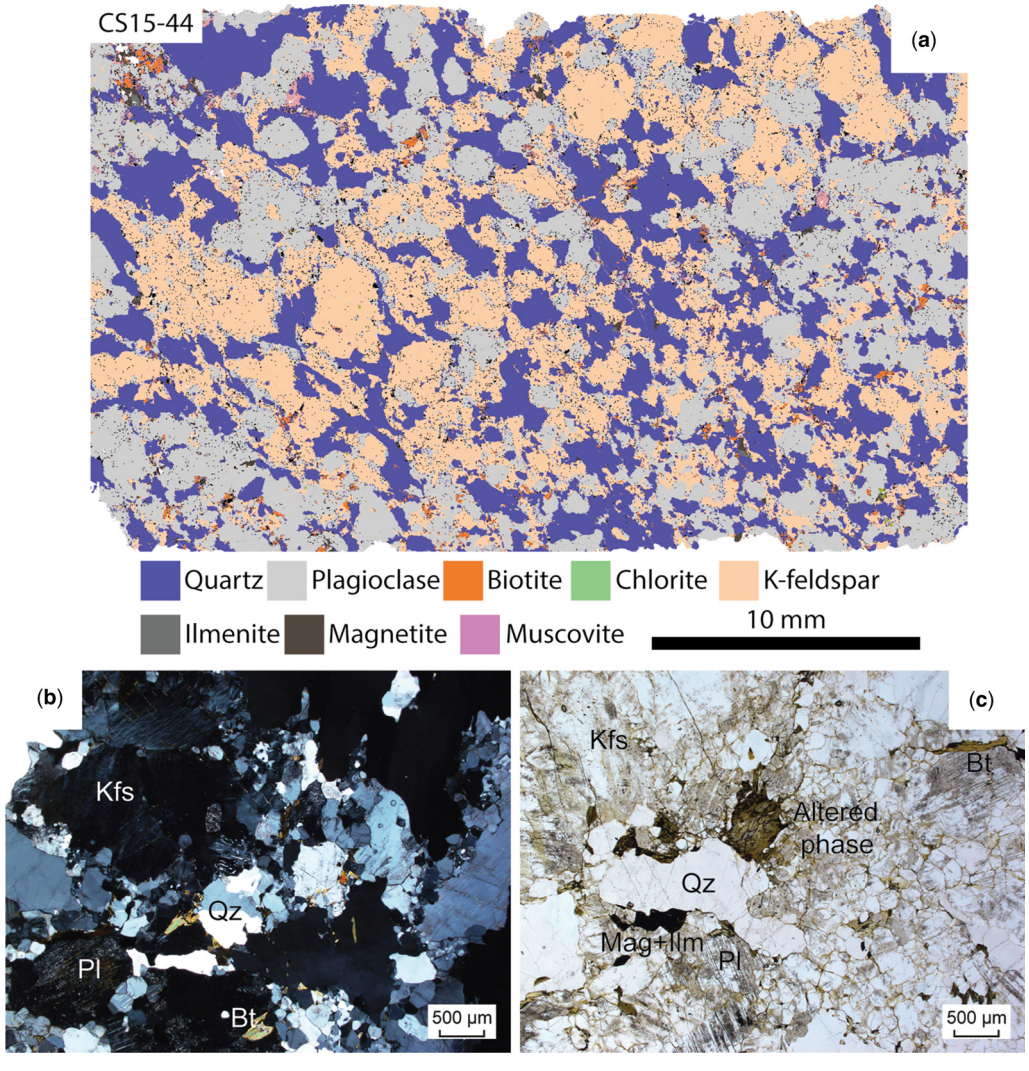

Fig. 3. (**a**) Tescan Integrated Mineral Analysis (TIMA) map of sample CS15-44 with a colour mineral legend. (**b**) and (**c**) Photomicrographs of CS15-44.

Monazite geochronology

Monazite from samples CS15-44 and CS15-49 were investigated *in situ* from within the matrix, within garnet where it was available and large enough to analyse, as well as near the margins of garnet. Monazite from both samples showed no visible zoning under BSE imaging (BSE) (Fig. 7d).

LA-ICP-MS analysis of monazite cores from the Quha and Leisure Bay formations (CS15-44 and CS15-49, respectively) yielded single populations for both samples (Fig. 8a). Monazite from the Quha Formation (CS15-44) had a weighted mean $^{207}Pb/^{206}Pb$ age of 987.4 ± 8.1 Ma (±21.3 Ma systematic uncertainty, $n = 25$, MSWD = 0.8), with monazite from the Leisure Bay Formation (CS15-49) having an older weighted mean age of 1032.7 ± 4.7 Ma (±21.2 Ma systematic uncertainty, $n = 9$, MSWD = 0.8) (Fig. 8b).

Phase equilibrium modelling

Compositional layering was observed within sample CS15-50 (Fig. 4b). However, an investigation of major elements (EPMA) and trace elements (LA-ICP-MS) within garnet from different compositional layers demonstrated that CS15-50, as well as

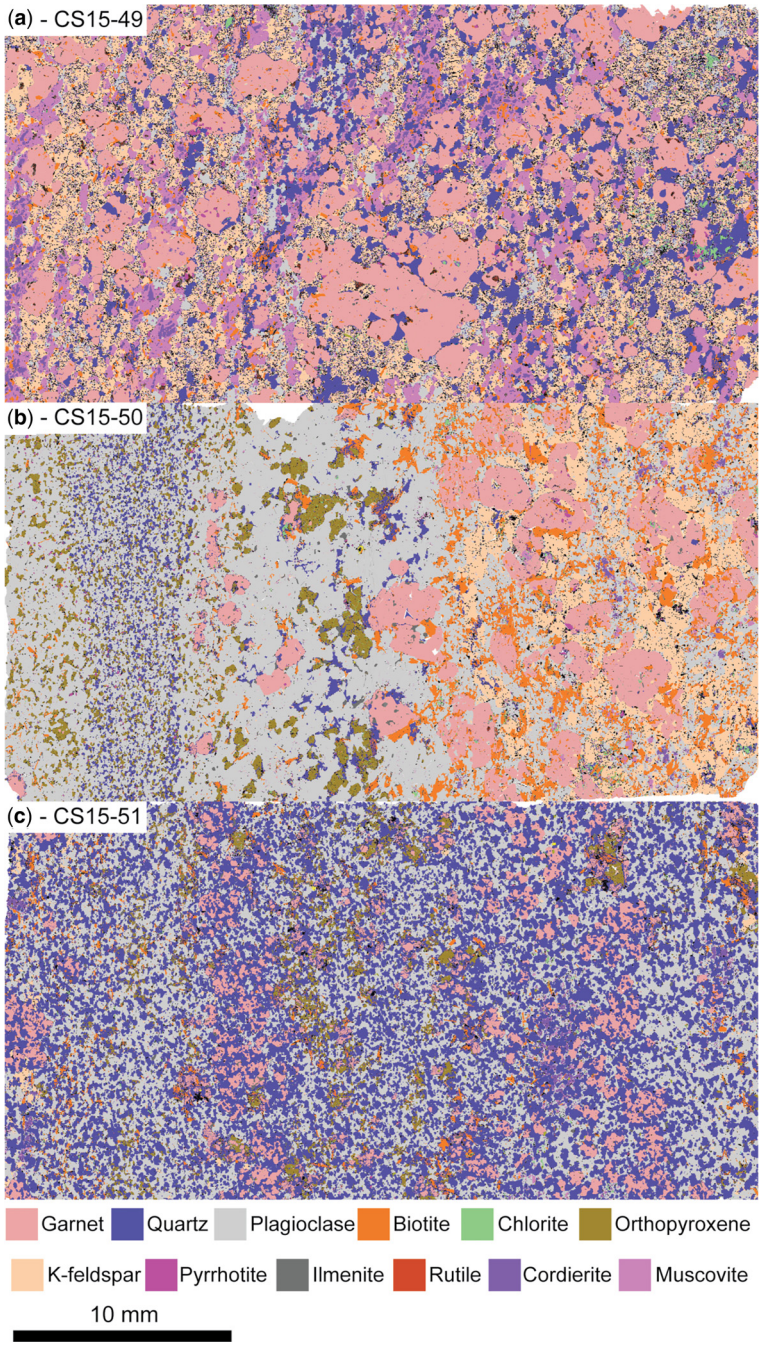

Fig. 4. Tescan Integrated Mineral Analysis (TIMA) map of samples CS15-49–CS15-51 with a colour mineral legend.

CS15-49, showed no significant compositional zoning within garnet or compositional changes across the thin section within all layers, indicating that the equilibration volume and diffusivity of elements within the sample was sufficient for the sample to equilibrate on at least the thin-section scale. As a

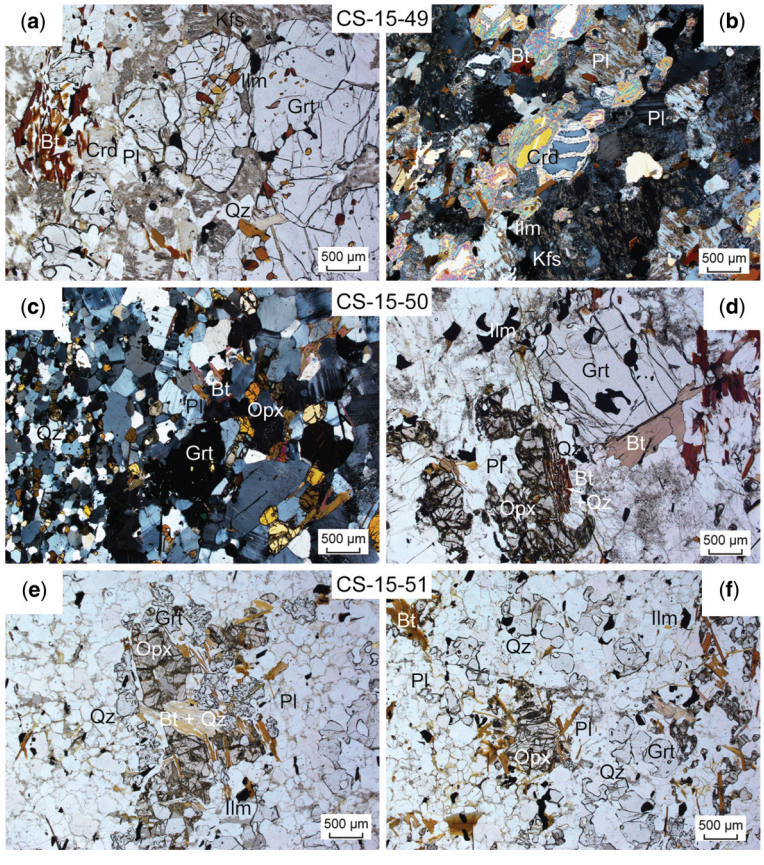

Fig. 5. (**a**) and (**b**) Photomicrographs of sample CS15-49. (**c**) and (**d**) Photomicrographs of sample CS15-50. (**e**) and (**f**) Photomicrographs of sample CS15-51.

result, bulk-rock compositions from material containing all recognized layers were used for the purpose of phase equilibrium modelling, over domain-based compositions.

Mzumbe Terrane. In the *P–T* pseudosection for sample CS15-44 (Fig. 9a) the solidus for the modelled H_2O content lies between 750 and 790°C. The interpreted peak assemblage of garnet, biotite, plagioclase, K-feldspar, quartz, magnetite, ilmenite and melt is predicted to have been between 3.9 and 7.8 kbar at 780–834°C (Fig. 9a). The peak assemblage is limited by the loss of magnetite above *c.* 7 kbar, as well as the growth of orthopyroxene at higher temperatures and cordierite at lower pressures than the peak assemblage.

Margate Terrane. In the *P–T* pseudosection for sample CS15-49 (Fig. 9b) the solidus for the modelled H_2O content lies between 800 and 830°C. The interpreted peak assemblage of garnet, cordierite, K-feldspar, quartz, ilmenite and melt occurred within a restricted *P–T* window between 5.5 and 6.4 kbar at 827–910°C. Sillimanite is stable at higher temperatures and pressures than the peak assemblage, with spinel stable at higher temperatures and magnetite stable at lower pressures. A small proportion of biotite can be grown just before crossing the solidus, consistent with the petrogenesis of the sample.

In the *P–T* pseudosection for sample CS15-50 (Fig. 9c) the solidus for the modelled H_2O content lies between 840 and 876°C. The interpreted peak assemblage of garnet, orthopyroxene, cordierite, biotite, plagioclase, K-feldspar, ilmenite and melt occurred between 5.5 and 6.5 kbar at 841–892°C. Cordierite is consumed up-temperature of the peak field, with the growth of spinel occurring at high temperatures and magnetite at low pressures. A small amount of quartz forms just before crossing the solidus, consistent with the minor amount of quartz in the sample.

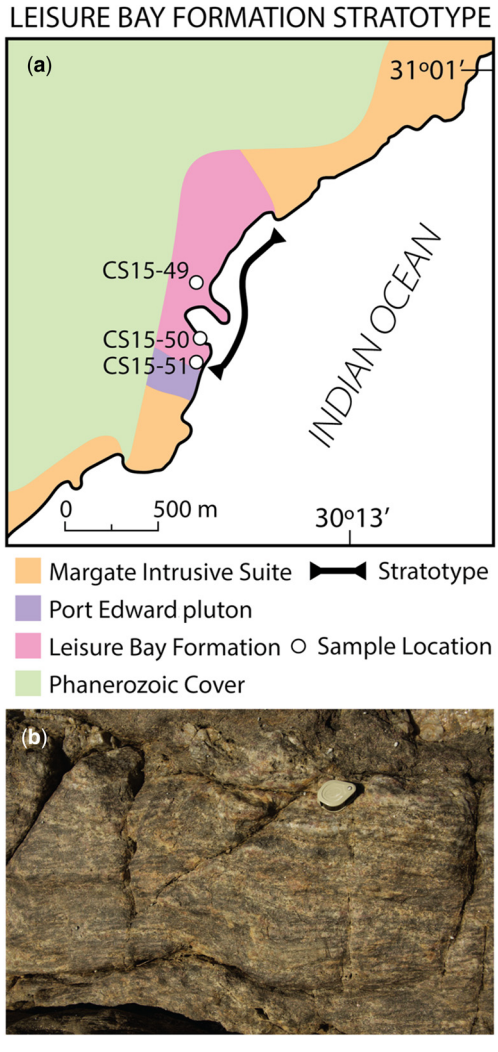

Fig. 6. (**a**) Simplified geological map of the Leisure Bay Formation stratotype showing the sample locations. (**b**) Field photograph of the pelitic gneisses of the Leisure Bay Formation with irregular garnet-bearing leucosomes. Garnet is also present within the melanosome. The hand lens is for scale.

In the *P–T* pseudosection for sample CS15-51 (Fig. 9d) the solidus lies at *c.* 850°C above a pressure of *c.* 6 kbar, with an inflection to *c.* 900°C below *c.* 6 kbar due to the loss of biotite and the presence of cordierite, with some H_2O partitioning into cordierite at lower pressures instead of partial melt. The interpreted peak assemblage of garnet, orthopyroxene, cordierite, plagioclase, K-feldspar, quartz, ilmenite and melt occurs between 5.1 and 6.1 kbar at 850–962°C. The sample grew a small portion of biotite before crossing the solidus, consistent with the petrology of the sample.

Discussion

Revised *P–T* conditions

For the Mzumbe Terrane our new *P–T* work is largely comparable to previous estimates (Evans *et al.* 1987). The psammitic sample from the Quha Formation (CS15-44) yielded *P–T* conditions between 780 and 834°C at 3.9–7.8 kbar. These conditions are *c.* 30°C more elevated than previous estimates (750–800°C at 6–8 kbar: Evans *et al.* 1987) with similar to lower pressures predicted. We saw no textural evidence for the growth of orthopyroxene and/or cordierite or the loss of magnetite that could limit our peak assemblage; however, we are unable to confirm the nature of the *P–T* path at this time due to the simplicity of the mineral paragenesis. Based on previous work (Evans *et al.* 1987), the psammitic assemblages of the Quha Formation are likely to have followed a typical clockwise *P–T* path (Fig. 9e; see also Figs 2 & 9a). We were unable to differentiate between a cooling path with moderate decompression and one with isobaric cooling due to limited pressure constraints (Fig. 9e). Mineral modes did not provide any additional refinement to our *P–T* constraints as none of the minerals stable within our peak assemblage had mineral modes that varied significantly with pressure, which is the broadest variable of our assemblage.

Unlike the Mzumbe Terrane, our *P–T* work in the Margate Terrane significantly refines existing *P–T* data. All three Leisure Bay samples share a field of overlap within the *P–T* space between 850 and 892°C at 5.7–6.1 kbar (Fig. 9e), vastly refined from previous estimates from mineral pair thermometry for M_1 and falling at more elevated pressures than previously recorded for M_1 (434–1100°C at *c.* 4 kbar: Mendonidis and Grantham 2003). Temperatures are similar to those previously reported from *P–T* grids for M_1 but, again, more refined (>850°C: Mendonidis and Grantham 2003). The conditions for our samples also include lower pressures for M_2 (7–9 kbar: Mendonidis and Grantham 2003). Whilst all three of our Leisure Bay samples overlap to some degree in the *P–T* space, there also appears to be a potential relationship between the maximum peak metamorphic temperature recorded and the distance of the sample from the Port Edward pluton (Oribi Gorge Suite, 1034.4 ± 0.6 Ma: Spencer *et al.* 2015) but not the Nicholson's Point granite (Margate Granite Suite, 1084.4 ± 1.7 Ma: Spencer *et al.* 2015), which are located on either side of the sample transect. The recorded peak temperature range increases between samples along the transect, with the most elevated temperatures experienced by

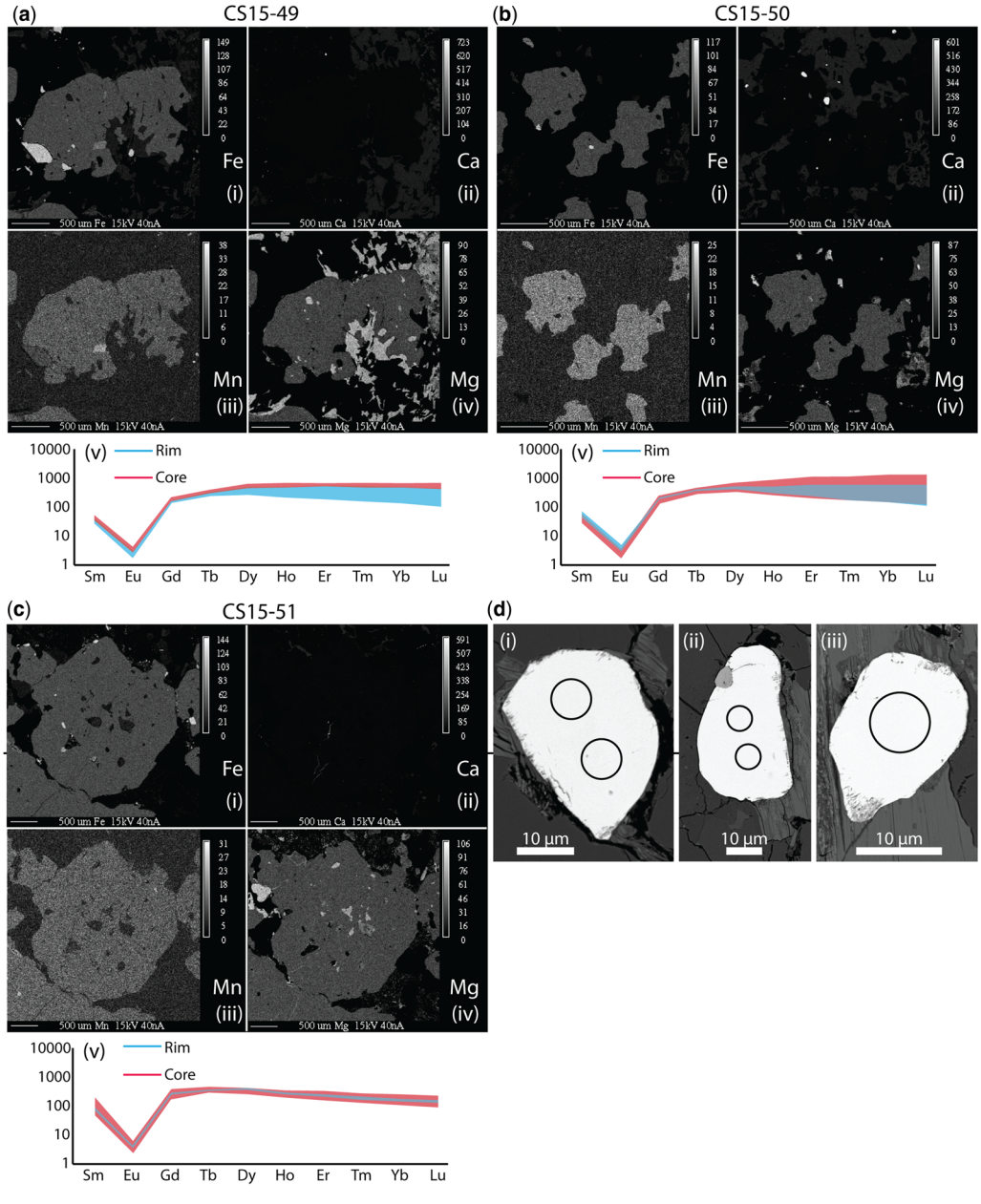

Fig. 7. (**a**) Garnet EPMA X-ray maps for (i–iv) major elements and (v) chondrite-normalized LA-ICP-MS trace elements from sample CS15-49. (**b**) Garnet EPMA X-ray maps for (i–iv) major elements and (v) LA-ICP-MS trace elements from sample CS15-50. (**c**) Garnet EPMA X-ray maps for (i–iv) major elements and (v) chondrite-normalized LA-ICP-MS trace elements from sample CS15-51. (**d**) (i–iii) Backscattered electron (BSE) images of monazite from sample CS15-49 that are representative of monazite in all samples.

sample CS15-51 (850–962°C), which is within 1 m of the Port Edward pluton, and the lowest temperature experienced by CS15-49 (827–910°C), which is the most removed from the Port Edward pluton (*c.* 50 m from the Nicholson's Point granite). The samples, which are up to 500 m apart, seemed to have followed similar *P–T* paths with slight changes in overall maximum temperature along the short

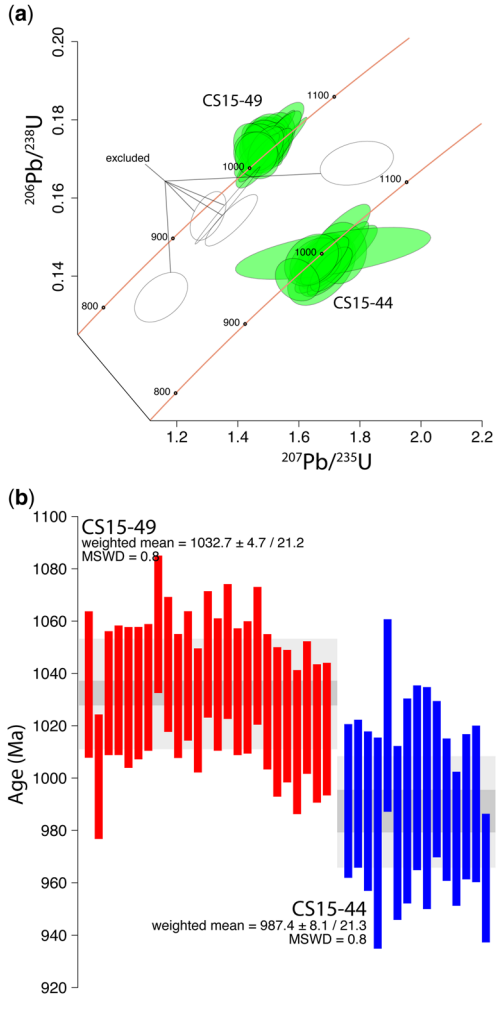

Fig. 8. (**a**) Wetherill concordia plot of laser ablation split-stream (LASS) U–Pb monazite ages from samples CS15-44 (Quha) and CS15-49 (Leisure Bay). (**b**) Weighted mean $^{207}Pb/^{206}Pb$ ages (with 2σ and systematic errors) for samples CS15-44 and CS15-49.

transect. This potentially indicates a relationship between peak metamorphism and the emplacement of the Oribi Gorge Suite, a point we will return to in the following subsection with regard to the age of metamorphism.

All three Leisure Bay samples followed a tight clockwise *P–T* path, followed by effectively isobaric cooling due to the limited stability field of the modelled assemblage as a result of a number of phase changes at higher *P* and/or *T*. These constraints at higher pressures are the loss of cordierite (CS15-50) and orthopyroxene (CS15-51), and the growth of sillimanite (CS15-49) (Fig. 9e), as well as the growth of spinel and magnetite at higher temperatures and lower pressures, respectively, both of which are absent in all samples. The essentially isobaric *P–T* path in this study's samples is consistent with previous studies (Grantham *et al.* 1994; Mendonidis and Grantham 2003) but is much more refined in terms of overall *P–T* conditions. As all of the samples exhibit partial melting, we only infer the prograde history of the *P–T* path.

Unlike previous studies, we did not see any evidence of a second metamorphic event within our samples from the Leisure Bay Formation connected to additional garnet growth (Mendonidis and Grantham 2003), and we did not see a second population, texturally or geochemically (Figs 5 & 7). However, samples CS15-49 and CS15-50 did contain retrograde micas and should have been fertile for later metamorphism, unlike samples described in previous studies. This could potentially indicate local variation in metamorphic conditions across the Margate Terrane. Samples interpreted to contain a secondary metamorphic assemblage should be re-evaluated using modern methods.

Age of metamorphism

The timing of peak metamorphism of the Mzumbe and Margate terranes was constrained using monazite dating from supracrustal metamorphic rocks in the respective terranes. Monazite from the Leisure Bay Formation yielded a late Stenian age (1032.7 $\pm$ 4.7/21.2 Ma, age $\pm$ weighted uncertainty/systematic uncertainty) (Fig. 8), which is in line with previous monazite dating from the Turtle Bay Suite that lies within an enigmatic high-shear zone between the Margate and Mzumbe terranes (Spencer *et al.* 2015; Mendonidis and Armstrong 2016) and overlaps with the *c.* 1050–1030 Ma timing of the Oribi Gorge Suite that spans both terranes (Spencer *et al.* 2015) (Fig. 10). The similar monazite ages of the Leisure Bay Formation and Turtle Bay Suite imply that the Turtle Bay Suite is likely to have experienced metamorphism associated with the intrusion of the Oribi Gorge Suite.

Thomas *et al.* (1999) dated zircon rims from the Quha Formation that were interpreted to be metamorphic in origin with an age of 1065 $\pm$ 15 Ma. This age is a $^{207}Pb/^{206}Pb$ age but, given the age of the grains, this should have been be recorded as a $^{206}Pb/^{238}Pb$ age (Spencer *et al.* 2016), which shows the significant disruption in all of the analyses. The dating of these rims should be reattempted in order to verify and increase the precision of these rims. The earliest Neoproterozoic age of monazite from the Quha Formation of the Mzumbe Terrane (987.4 $\pm$ 8.1/21.3 Ma) (Fig. 8) is the youngest tectonomagmatic event confirmed with robust geochronology (cf. 951 $\pm$ 16 Ma Rb–Sr whole-rock

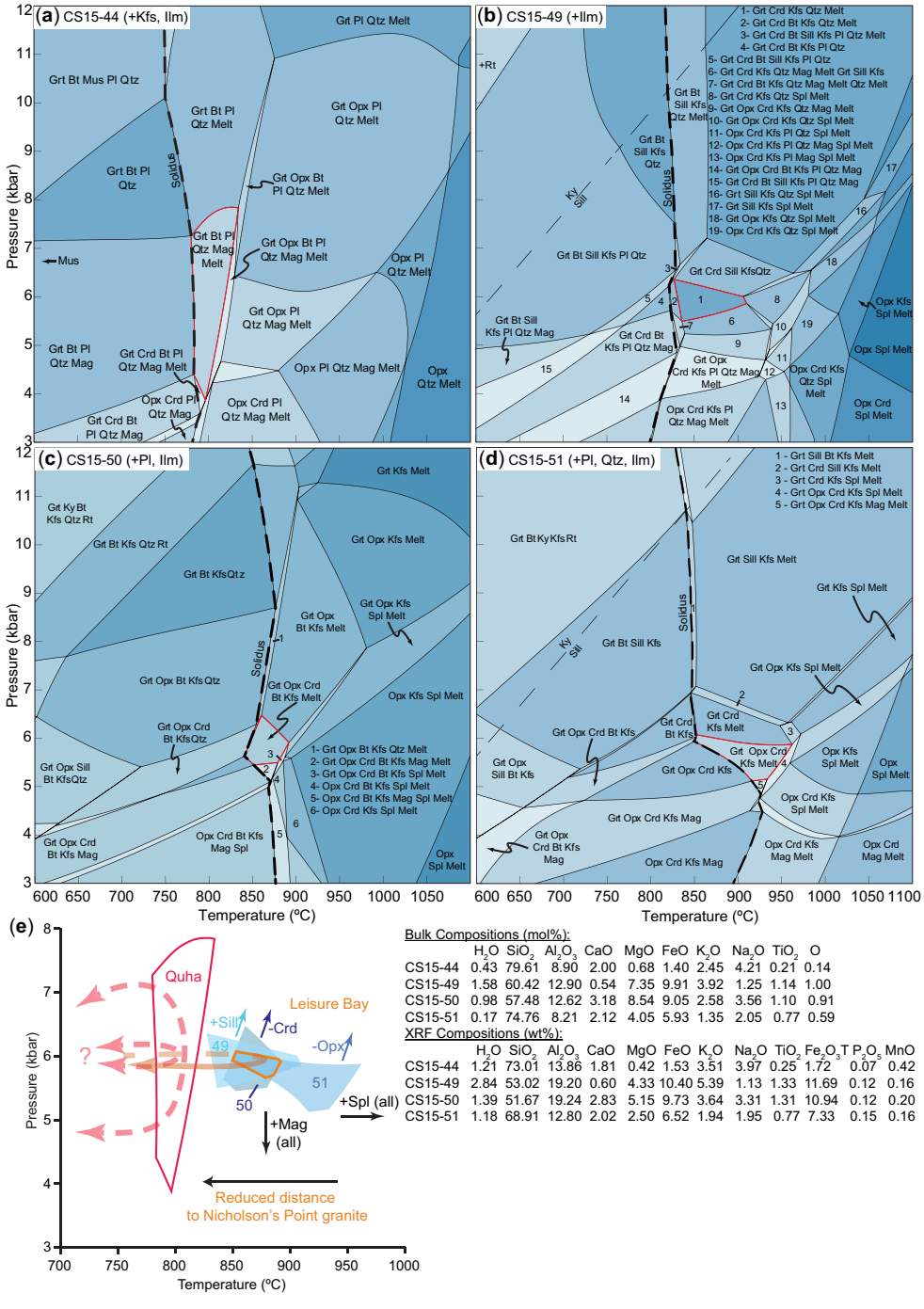

Bulk Compositions (mol%):

	H_2O	SiO_2	Al_2O_3	CaO	MgO	FeO	K_2O	Na_2O	TiO_2	O
CS15-44	0.43	79.61	8.90	2.00	0.68	1.40	2.45	4.21	0.21	0.14
CS15-49	1.58	60.42	12.90	0.54	7.35	9.91	3.92	1.25	1.14	1.00
CS15-50	0.98	57.48	12.62	3.18	8.54	9.05	2.58	3.56	1.10	0.91
CS15-51	0.17	74.76	8.21	2.12	4.05	5.93	1.35	2.05	0.77	0.59

XRF Compositions (wt%):

	H_2O	SiO_2	Al_2O_3	CaO	MgO	FeO	K_2O	Na_2O	TiO_2	Fe_2O_3T	P_2O_5	MnO
CS15-44	1.21	73.01	13.86	1.81	0.42	1.53	3.51	3.97	0.25	1.72	0.07	0.42
CS15-49	2.84	53.02	19.20	0.60	4.33	10.40	5.39	1.13	1.33	11.69	0.12	0.16
CS15-50	1.39	51.67	19.24	2.83	5.15	9.73	3.64	3.31	1.31	10.94	0.12	0.20
CS15-51	1.18	68.91	12.80	2.02	2.50	6.52	1.94	1.95	0.77	7.33	0.15	0.16

Fig. 9. *P–T* pseudosections of (**a**) sample CS15-44 from the Quha Formation, and (**b**) samples CS15-49, (**c**) CS15-50 and (**d**) CS15-51 from the Leisure Bay Formation. The solidus is highlighted by a black dashed line, with the interpreted peak assemblage outlined in red. (**e**) *P–T* summary diagram with potential *P–T* paths for both the Quha Formation (red) and Leisure Bay Formation (orange), and the field of overlap between the three Leisure Bay samples (CS15-49–CS15-51). Bulk compositions used in the modelled pseudosections are also listed in mol%, as well as original XRF bulk compositions in wt%.

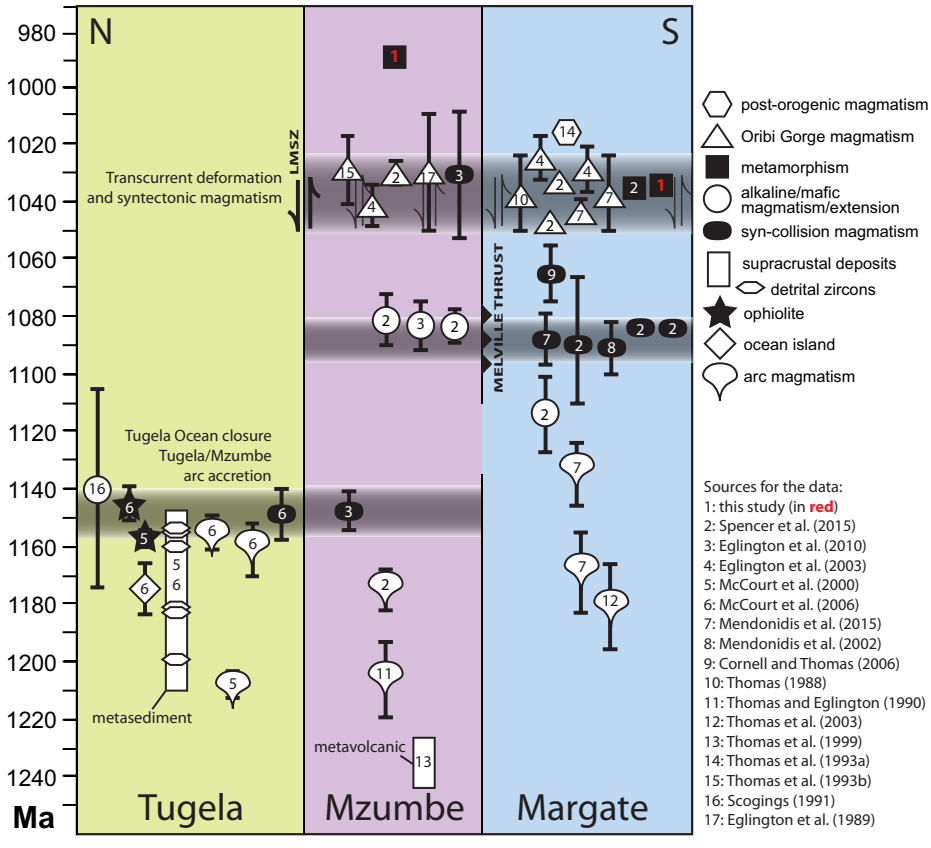

Fig. 10. Time–space diagram of the magmatic, sedimentary and metamorphic evolution of the whole Natal Belt, modified after Spencer *et al.* (2015).

isochron age of the Sezela Suite of alkaline igneous rocks: Eglington *et al.* 1989). Although there is overlap in the individual monazite ages from both of these units, both the weighted means using analytical uncertainties (a less conservative age estimate) and weighted means incorporating systematic uncertainties (a more conservative age estimate) are discrete with no overlapping uncertainties. Depending on whether the zircon rims of Thomas *et al.* (1999) can be verified, it is possible that the *c.* 987 Ma age of monazite could be post-peak crystallization or peak crystallization if the zircon does not represent a discrete population but instead resetting due to later metamorphism. It has been shown that monazite can grow without further or new zircon growth (Morrissey *et al.* 2016), so the lack of a zircon population of this age is possible. However, the difference in metamorphic age of the supracrustals from the two terranes implies that they experienced different metamorphic events in terms of timing and potentially duration.

Impacts on the tectonic history of the Natal Belt

Previous models posit that accretion of the Tugela, Mzumbe and Margate terranes proceeded from north to south with accretion of the Tugela and Mzumbe terranes, with the Kaapvaal cratonic margin occurring at *c.* 1150 Ma (McCourt *et al.* 2006; Spencer *et al.* 2015). The Margate Terrane is then thought to have accreted at *c.* 1100–1090 Ma (Eglington *et al.* 2003; Mendonidis *et al.* 2015; Spencer *et al.* 2015). The young age of the monazite (*c.* 987 Ma) from the Quha Formation provides evidence that tectonism within the Mzumbe Terrane continued during protracted accretion into the earliest Neoproterozoic (Fig. 10). This may have been associated with further crustal thickening via oblique thrusting along the Melville Thrust that lies between the Mzumbe and Margate terranes (Jacobs and Thomas 1994). This hypothesis could be validated through the dating of deformation fabrics associated with the Melville Thrust. This *c.* 990 Ma monazite

age of the Quha Formation is not supportive of thermal perturbation due to the Oribi Gorge Suite intrusion as no Oribi Gorge Suite ages exist younger than *c.* 1000 Ma (Spencer *et al.* 2015). The isobaric cooling of the Margate Terrane may also provide a clue as to the duration of peak metamorphism, in that isobaric cooling would prolong high-grade metamorphic conditions more so than isothermal decompression during rapid exhumation. In addition, similarly aged magmatism is present in the Maurice Ewing Bank (undeformed granite at 1006 ± 13 Ma: Chemale *et al.* 2018), whose reconstructed Neoproterozoic position lies along the Natal margin of South Africa, indicating that metamorphism in the Mzumbe Terrane may also be related to magmatism; however, this is yet to be substantiated. The Sezela Suite is too old to explain the monazite ages reported herein (*c.* 1080 Ma: Spencer *et al.* 2015). Further work is needed to elucidate the spatial extent of this younger metamorphic event and any cryptic magmatism with which it may have been associated.

Conclusions

The Mzumbe Terrane experienced high-temperature–medium-pressure (HT–LP) metamorphism, reaching a peak of 780–834°C at 3.9–7.8 kbar but the post-peak evolution is unclear. The Margate Terrane experienced HT–LP metamorphism along an essentially isobaric *P–T* path but achieved higher temperature conditions of 850–892°C at 5.7–6.1 kbar. Previous studies have assumed coeval metamorphic histories for the Mzumbe and Margate terranes. We argue that the thermal peak of metamorphism in the Mzumbe Terrane (987.4 ± 8.1 Ma) post-dates similar grade and style of metamorphism in the Margate Terrane (1032.7 ± 4.7 Ma) by *c.* 40 myr, indicating that the metamorphic evolution of the Natal Belt is more complex than previously thought. Metamorphism in the Margate Terrane appears to have been tied to the *c.* 1030 Ma emplacement of the Oribi Gorge Suite, assumed using the age of metamorphic monazite and potential variation in peak temperature conditions between samples with distance from the Port Edward pluton. Metamorphism at *c.* 987 Ma in the Mzumbe Terrane may have been a product of additional thrusting along the Melville Thrust, although the event could potentially be related to magmatism; further study on this is required. These new data can be explained by advective cooling during orthogonal or oblique transcurrent deformation (Chen *et al.* 2015; Xu *et al.* 2015) that is supported by the oblique structural and tectonic features of the Natal Province (Jacobs and Thomas 1994), these features have yet to be dated directly. This model predicts isobaric cooling while minimizing exhumation and provides a possible explanation for the protracted nature of metamorphism in the NMP.

Acknowledgements Many thanks go to Noreen Evans and Brad McDonald for their assistance with the LA-ICP-MS analysis. We thank Mike Dorais for assistance in the XRF and electron microprobe analyses at Brigham Young University. We would also like to thank the reviewers of this paper.

Competing interests The authors declare that they have no known competing financial interests or personal relationships that could have appeared to influence the work reported in this paper.

Author contributions **EB**: conceptualization (supporting), data curation (equal), formal analysis (equal), investigation (equal), methodology (equal), writing – original draft (lead), writing – review & editing (equal); **CS**: conceptualization (lead), data curation (equal), formal analysis (equal), investigation (equal), methodology (equal), writing – original draft (supporting), writing – review & editing (equal).

Funding GeoHistory Facility instruments (part of the John de Laeter Centre) were funded via an Australian Geophysical Observing System (AGOS) grant provided to AuScope by the AQ44 Australian Education Investment Fund. The Australian Microscopy and Microanalysis Research Facility, AuScope, the Australian Science and Industry Endowment Fund, and the State Government of Western Australia contributed funding to the Centre for Microscopy, Characterization and Analysis at the University of Western Australia. The Tescan Integrated Mineral Analysis (TIMA) instrument at the John de Laeter Centre was funded by a grant from the Australian Research Council (LE140100150) and is operated with the support of the Geological Survey of Western Australia, University of Western Australia and Murdoch University.

Data availability All data generated or analysed during this study are included in this published article (and, if present, its supplementary information files).

References

Aleinikoff, J.N., Schenck, W.S., Plank, M.O., Srogi, L., Fanning, C.M., Kamo, S.L. and Bosbyshell, H. 2006. Deciphering igneous and metamorphic events in high-grade rocks of the Wilmington Complex, Delaware: Morphology, cathodoluminescence and backscattered electron zoning, and SHRIMP U–Pb geochronology of zircon and monazite. *Geological Society of America Bulletin*, **118**, 39–64, https://doi.org/10.1130/B25659.1

Anders, E. and Grevesse, N. 1989. Abundances of the elements: Meteoritic and solar. *Geochimica et Cosmochimica acta*, **53**, 197–214, https://doi.org/10.1016/0016-7037(89)90286-X

Blereau, E., Clark, C., Taylor, R.J.M., Johnson, T.E., Fitzsimons, I.C.W. and Santosh, M. 2016. Constraints on the timing and conditions of high-grade metamorphism, charnockite formation and fluid–rock interaction in the Trivandrum Block, southern India. *Journal of Metamorphic Geology*, **34**, 527–549, https://doi.org/10.1111/jmg.12192

Blereau, E., Johnson, T.E., Clark, C., Taylor, R.J.M., Kinny, P.D. and Hand, M. 2017. Reappraising the *P–T* evolution of the Rogaland–Vest Agder Sector, southwestern Norway. *Geoscience Frontiers*, **8**, 1–14, https://doi.org/10.1016/j.gsf.2016.07.003

Blereau, E., Clark, C. *et al*. 2019. Closed system behaviour of argon in osumilite records protracted high-temperature metamorphism within the Rogaland-Vest Agder Sector, Norway. *Journal of Metamorphic Geology*, **37**, 667–680, https://doi.org/10.1111/jmg.12480

Blereau, E., Clark, C., Kinny, P.D., Sansom, E., Taylor, R.J.M. and Hand, M. 2022. Probing the history of ultra-high temperature metamorphism through rare earth element diffusion in zircon. *Journal of Metamorphic Geology*, **40**, 329–357, https://doi.org/10.1111/jmg.12630

Carvalho, B.B., Bartoli, O. *et al.* 2019. Anatexis and fluid regime of the deep continental crust: New clues from melt and fluid inclusions in metapelitic migmatites from Ivrea Zone (NW Italy). *Journal of Metamorphic Geology*, **37**, 951–975, https://doi.org/10.1111/jmg.12463

Chemale, F., Ramos, V.A., Naipauer, M., Girelli, T.J. and Vargas, M. 2018. Age of basement rocks from the Maurice Ewing Bank and the Falkland/Malvinas Plateau. *Precambrian Research*, **314**, 28–40, https://doi.org/10.1016/j.precamres.2018.05.026

Chen, X., Liu, J., Tang, Y., Song, Z. and Cao, S. 2015. Contrasting exhumation histories along a crustal-scale strike-slip fault zone: The Eocene to Miocene Ailao Shan-River shear zone in southeastern Tibet. *Journal of Asian Earth Sciences*, **144**, 174–187, https://doi.org/10.1016/j.jseaes.2015.05.020

Clark, C., Taylor, R.J.M., Kylander-Clark, A.R.C. and Hacker, B.R. 2018. Prolonged (>100 Ma) ultrahigh temperature metamorphism in the Napier Complex, East Antarctica: A petrochronological investigation of Earth's hottest crust. *Journal of Metamorphic Geology*, **36**, 1117–1139, https://doi.org/10.1111/jmg.12430

Cornell, D.H. and Thomas, R.J. 2006. Age and tectonic significance of the Banana Beach gneiss, KwaZulu-Natal south coast, *South Africa*. *South African Journal of Geology*, **109**, 335–340, https://doi.org/10.2113/gssajg.109.3.335

Eglington, B.M., Harmer, R.E. and Kerr, A. 1989. Isotope and geochemical constraints on Proterozoic crustal evolution in south-eastern Africa. *Precambrian Research*, **45**, 159–174, https://doi.org/10.1016/0301-9268(89)90037-5

Eglington, B.M., Thomas, R.J., Armstrong, R.A. and Walraven, F. 2003. Zircon geochronology of the Oribi Gorge Suite, KwaZulu-Natal, South Africa: constraints on the timing of trans-current shearing in the Namaqua–Natal Belt. *Precambrian Research*, **123**, 29–46, https://doi.org/10.1016/S0301-9268(03)00016-0

Eglington, B.M., Thomas, R.J. and Armstrong, R.A. 2010. U–Pb SHRIMP zircon dating of Mesoproterozoic magmatic rocks from the Scottburgh Area, central Mzumbe terrane, KwaZulu-Natal, South Africa. *South African Journal of Geology*, **113**, 229–235, https://doi.org/10.2113/gssajg.113.2.229

Engi, M., Lanari, P. and Kohn, M.J. 2017. Significant ages – An introduction to petrochronology. *Reviews in Mineralogy and Geochemistry*, **83**, 1–12, https://doi.org/10.2138/rmg.2017.83.1

Evans, E.P., Eglington, B.M., Kerr, A. and Saggerson, E.P. 1987. The geology of the Proterozoic rocks around Umzinto, southern Natal, South Africa. *South African Journal of Geology*, **90**, 471–488.

Evans, M.J. 1984. *Precambrian Geology West of Scottburgh, Natal*. MSc dissertation, University of Natal, Durban, South Africa.

Grantham, G.H. 1983. *The Tectonic, Metamorphic and Intrusive History of the Natal Mobile Belt between Glenmore and Port Edward, Natal*. MSc dissertation, University of Natal, Durban, South Africa.

Grantham, G.H., Thomas, R.J. and Mendonidis, P. 1991. Leisure Bay Formation. *In*: *Catalogue of South African Lithostratigraphic Units, Volume 3*. Government Printer for the South African Committee for Stratigraphy, Pretoria, 17–18.

Grantham, G.H., Thomas, R.J., Eglington, B.M., De Bruin, D., Atanasov, A. and Evans, M.J. 1993. Corona textures in Proterozoic olivine melanorites of the Equeefa Suite, Natal metamorphic province, South Africa. *Mineralogy and Petrology*, **49**, 91–102, https://doi.org/10.1007/BF01162928

Grantham, G.H., Thomas, R.J. and Mendonidis, P. 1994. Contrasting P–T–t loops from southern East Africa, Natal and East Antarctica. *Journal of African Earth Sciences*, **19**, 225–235, https://doi.org/10.1016/0899-5362(94)90062-0

Grantham, G.H., Mendonidis, P., Thomas, R.J. and Satish-Kumar, M. 2012. Multiple origins of charnockite in the Mesoproterozoic Natal belt, Kwazulu-Natal, South Africa. *Geoscience Frontiers*, **3**, 755–771, https://doi.org/10.1016/j.gsf.2012.05.006

Green, E.C.R., White, R.W., Diener, J.F.A., Powell, R., Holland, T.J.B. and Palin, R.M. 2016. Activity–composition relations for the calculation of partial melting equilibria in metabasic rocks. *Journal of Metamorphic Geology*, **34**, 845–869, https://doi.org/10.1111/jmg.12211

Guiraud, M., Holland, T. and Powell, R. 1990. Calculated mineral equilibria in the greenschist–blueschist–eclogite facies in Na_2O–FeO–MgO–Al_2O_3–SiO_2–H_2O. *Contributions to Mineralogy and Petrology*, **104**, 85–98, https://doi.org/10.1007/BF00310648

Holder, R.M., Hacker, B.R., Kylander-Clark, A.R.C. and Cottle, J.M. 2015. Monazite trace-element and isotopic signatures of (ultra)high-pressure metamorphism: Examples from the Western Gneiss Region, Norway. *Chemical Geology*, **409**, 99–111, https://doi.org/10.1016/j.chemgeo.2015.04.021

Holland, T.J.B. and Powell, R. 2011. An improved and extended internally consistent thermodynamic dataset for phases of petrological interest, involving a new equation of state for solids. *Journal of Metamorphic Geology*, **29**, 333–383, https://doi.org/10.1111/j.1525-1314.2010.00923.x

Horstwood, M.S.A., Košler, J. *et al*. 2016. Community-derived standards for LA-ICP-MS U–(Th–)Pb

geochronology – uncertainty propagation, age interpretation and data reporting. *Geostandards and Geoanalytical Research*, **40**, 311–332, https://doi.org/10.1111/j.1751-908X.2016.00379.x

Jacobs, J. and Thomas, R.J. 1994. Oblique collision at about 1.1 Ga along the southern margin of the Kaapvaal continent, south-east Africa. *Geologische Rundaschau*, **83**, 322–333, https://doi.org/10.1007/BF00210548

Johnson, T., Clark, C., Taylor, R., Santosh, M. and Collins, A.S. 2015. Prograde and retrograde growth of monazite in migmatites: An example from the Nagercoil Block, southern India. *Geoscience Frontiers*, **6**, 373–387, https://doi.org/10.1016/j.gsf.2014.12.003

Kohn, M.J. 2016. Metamorphic chronology – a tool for all ages: Past achievements and future prospects. *American Mineralogist*, **101**, 25–42, https://doi.org/10.2138/am-2016-5146

Kylander-Clark, A.R.C., Hacker, B.R. and Cottle, J.M. 2013. Laser-ablation split-stream ICP petrochronology. *Chemical Geology*, **345**, 99–112, https://doi.org/10.1016/j.chemgeo.2013.02.019

Laurent, A.T., Bingen, B., Duchene, S., Whitehouse, M.J., Seydoux-Guillaume, A.-M. and Bosse, V. 2018*a*. Decoding a protracted zircon geochronological record in ultrahigh temperature granulite, and persistence of partial melting in the crust, Rogaland, Norway. *Contributions to Mineralogy and Petrology*, **173**, 29, https://doi.org/10.1007/s00410-018-1455-4

Laurent, A.T., Duchene, S., Bingen, B., Bosse, V. and Seydoux-Guillaume, A.-M. 2018*b*. Two successive phases of ultrahigh temperature metamorphism in Rogaland, S. Norway: evidence from Y-in-monazite thermometry. *Journal of Metamorphic Geology*, **36**, 1009–1037, https://doi.org/10.1111/jmg.12425

Lindsley, D.H. 1983. Pyroxene thermometry. *American Mineralogist*, **68**, 477–493.

McCourt, S., Bisnath, A. *et al*. 2000. Geology and tectonic setting of the Tugela Terrane, Natal Belt, South Africa. *Journal of African Earth Sciences*, **31**, Suppl. 1, 48–49, https://doi.org/10.1016/S0899-5362(00)00050-6

McCourt, S., Armstrong, R.A., Grantham, G.H. and Thomas, R.J. 2006. Geology and evolution of the Natal belt, South Africa. *Journal of African Earth Sciences*, **46**, 71–92, https://doi.org/10.1016/j.jafrearsci.2006.01.013

Mendonidis, P. and Grantham, G.H. 2003. Petrology, origin and metamorphic history of Proterozoic-aged granulites of the Natal Metamorphic Province, southeastern Africa. *Gondwana Research*, **6**, 607–628, https://doi.org/10.1016/S1342-937X(05)71011-X

Mendonidis, P. and Armstrong, R.A. 2016. U–Pb Zircon (SHRIMP) ages of granite sheets and timing of deformational events in the Natal Metamorphic Belt, southeastern Africa: Evidence for deformation partitioning and implications for Rodinia reconstructions. *Precambrian Research*, **278**, 22–33.

Mendonidis, P. and Thomas, R.J. 2019. A review of the geochronology of the Margate Terrane reveals a history of diachronous terrane docking and arc accretion across the Mesoproterozoic Natal belt, southeastern Africa. *Journal of African Earth Sciences*, **150**, 532–545, https://doi.org/10.1016/j.jafrearsci.2018.07.021

Mendonidis, P., Armstrong, R., Eglington, B.M., Grantham, G.H. and Thomas, R.J. 2002. Metamorphic history and U–Pb Zircon (SHRIMP) geochronology of the Glenmore Granite: implications for the tectonic evolution of the Natal Metamorphic Province. *South African Journal of Geology*, **105**, 325–336, https://doi.org/10.2113/1050325

Mendonidis, P., Thomas, R.J., Grantham, G.H. and Armstrong, R.A. 2015. Geochronology of emplacement and charnockite formation of the Margate Granite Suite, Natal Metamorphic Province, South Africa: Implications for Natal–Maud belt correlations. *Precambrian Research*, **265**, 189–202, https://doi.org/10.1016/j.precamres.2015.02.013

Morrissey, L.J., Hand, M., Kelsey, D.E. and Wade, B.P. 2016. Cambrian high-temperature reworking of the Rayner–Eastern Ghats terrane: Constraints from the northern Prince Charles Mountains region, East Antarctica. *Journal of Petrology*, **57**, 53–92, https://doi.org/10.1093/petrology/egv082

Paton, C., Woodhead, J., Hellstrom, J., Hergt, J., Greig, A. and Maas, R. 2010. Improved laser ablation U–Pb zircon and geochronology through robust downhole fractionation correction. *Geochemistry, Geophysics, Geosystems*, **11**, 1–36, https://doi.org/10.1029/2009GC002618

Paton, C., Hellstrom, J., Paul, B., Woodhead, J. and Hergt, J. 2011. Iolite: freeware for the visualisation and processing of mass spectrometric data. *Journal of Analytical Atomic Spectrometry*, **26**, 2508–2518, https://doi.org/10.1039/c1ja10172b

Pearce, N.J.G., Perkins, W.T., Westgate, J.A., Gorton, M.P., Jackson, S.E., Neal, C.R. and Chenery, S.P. 1997. A compilation of new and published major and trace element data for NIST SRM 610 and NIST SRM 612 glass reference materials. *Geostandards Newsletter*, **21**, 115–144, https://doi.org/10.1111/j.1751-908X.1997.tb00538.x

Powell, R. and Holland, T.J.B. 1988. An internally consistent thermodynamic dataset with uncertainties and correlations: 3. Application, methods and worked examples and a computer program. *Journal of Metamorphic Geology*, **6**, 173–204, https://doi.org/10.1111/j.1525-1314.1988.tb00415.x

Rubatto, D. 2017. Zircon: the metamorphic mineral. *Reviews in Mineralogy and Geochemistry*, **83**, 261–295, https://doi.org/10.2138/rmg.2017.83.9

Scogings, A.J. 1991. *Alkaline Intrusives from the Tugela Terrane, Natal Metamorphic Province*. PhD thesis, University of Durban-Westville, Westville, Durban, South Africa, http://hdl.handle.net/10413/11162

Spencer, C.J., Thomas, R.J., Roberts, N.M.W., Cawood, P.A., Millar, I. and Tapster, S. 2015. Crustal growth during island arc accretion and transcurrent deformation, Natal Metamorphic Province, South Africa: new isotopic constraints. *Precambrian Research*, **265**, 203–217, https://doi.org/10.1016/j.precamres.2015.05.011

Spencer, C.J., Kirkland, C.L. and Taylor, R.J.M. 2016. Strategies towards statistically robust interpretations of *in situ* U–Pb zircon geochronology. *Geoscience Frontiers*, **7**, 581–589, https://doi.org/10.1016/j.gsf.2015.11.006

Spencer, C.J., Yakymchuk, C. and Ghaznavi, M. 2017. Visualising data distributions with kernel density estimation and reduced chi-squared statistic. *Geoscience*

Frontiers, **8**, 1247–1252, https://doi.org/10.1016/j.gsf.2017.05.002

Taylor, R.J.M., Clark, C., Fitzsimons, I.C.W., Santosh, M., Hand, M., Evans, N. and McDonald, B. 2014. Post-peak, fluid-mediated modification of granulite facies zircon and monazite in the Trivandrum Block, southern India. *Contributions to Mineralogy and Petrology*, **168**, 1044, https://doi.org/10.1007/s00410-014-1044-0

Taylor, R.J.M., Kirkland, C.L. and Clark, C. 2016. Accessories after the facts: Constraining the timing, duration and conditions of high-temperature metamorphic processes. *Lithos*, **264**, 239–257, https://doi.org/10.1016/j.lithos.2016.09.004

Taylor, R.J.M., Clark, C., Harley, S.L., Kylander-Clark, A.R.C., Hacker, B.R. and Kinny, P.D. 2017. Interpreting granulite facies events through rare earth element partitioning arrays. *Journal of Metamorphic Geology*, **35**, 759–775, https://doi.org/10.1111/jmg.12254

Thomas, R.J. 1988. *The Geology of the Port Shepstone Area. Explanation of Sheet 3030 Port Shepstone*. Geological Survey of South Africa, Johannesburg, South Africa.

Thomas, R.J. 1989. A tale of two tectonic terranes. *South African Journal of Geology*, **92**, 306–321.

Thomas, R.J. 1990. Mzumbe Gneiss Suite. *In*: *Catalogue of South African Lithostratigraphic Units, Volume 2*. Government Printer for the South African Committee for Stratigraphy, Pretoria, 35–36.

Thomas, R.J. 1992*a*. Mapumulo Group. *In*: *Catalogue of South African Lithostratigraphic Units, Volume 4*. Government Printer for the South African Committee for Stratigraphy, Pretoria, 11–14.

Thomas, R.J. 1992*b*. Mzimkulu Group. *In*: *Catalogue of South African Lithostratigraphic Units, Volume 4*. Government Printer for the South African Committee for Stratigraphy, Pretoria, 17–18.

Thomas, R.J. and Eglington, B.M. 1990. A Rb–Sr, Sm–Nd and U–Pb zircon isotopic study of the Mzumbe Suite, the oldest intrusive granitoid in southern Natal, South Africa. *South African Journal of Geology*, **93**, 761–765.

Thomas, R.J., Evans, M.J. and Eglington, B.M. 1991*a*. Equeefa Suite. *In*: *Catalogue of South African Lithostratigraphic Units, Volume 3*. Government Printer for the South African Committee for Stratigraphy, Pretoria, 9–12.

Thomas, R.J., Evans, M.J. and Eglington, B.M. 1991*b*. Quha Formation. *In*: *Catalogue of South African Lithostratigraphic Units, Volume 3*. Government Printer for the South African Committee for Stratigraphy, Pretoria, 41–44.

Thomas, R.J., Mendonidis, P., Grantham, G.H. and Johnson, M.R. 1991*c*. Margate Granite Suite. *In*: *Catalogue of South African Lithostratigraphic Units, Volume 3*. Government Printer for the South African Committee for Stratigraphy, Pretoria, 33–36.

Thomas, R.J., Ashwal, L.D. and Andreoli, M.A.G. 1992*a*. The petrology of the Turtle Bay Suite: a mafic–felsic granulite association from southern Natal, South Africa. *Journal of African Earth Sciences (and the Middle East)*, **15**, 187–206, https://doi.org/10.1016/0899-5362(92)90068-N

Thomas, R.J., Eglington, B.M., Evans, M.J. and Kerr, A. 1992*b*. The petrology of the Proterozoic Equeefa Suite, southern Natal, South Africa. *South African Journal of Geology*, **95**, 116–130.

Thomas, R.J., Eglington, B.M. and Bowring, S.A. 1993*a*. Dating the cessation of Kibaran magmatism in Natal, South Africa. *Journal of African Earth Science (and the Middle East)*, **16**, 247–252, https://doi.org/10.1016/0899-5362(93)90046-S

Thomas, R.J., Eglington, B.M., Bowring, S.A., Retief, E.A. and Walraven, F. 1993*b*. New isotope data from a neoproterozoic porphyritic garnitoid–charnockite suite from Natal, South Africa. *Precambrian Research*, **62**, 83–101, https://doi.org/10.1016/0301-9268(93)90095-J

Thomas, R.J., Cornell, D.H. and Armstrong, R.A. 1999. Provenance age and metamorphic history of the Quha Formation, Natal Metamorphic Province: a U–Th–Pb zircon SHRIMP study. *South African Journal of Geology*, **102**, 83–88.

Thomas, R.J., Armstrong, R.A. and Eglington, B.M. 2003. Geochronology of the Sikombe Granite, Transkei, Natal Metamorphic Province, South Africa. *South African Journal of Geology*, **106**, 403–408, https://doi.org/10.2113/106.4.403

Tomascak, P.B., Krogstad, E.J. and Walker, R.J. 1996. U–Pb monazite geochronology of granitic rocks from Maine: Implications for Late Paleozoic tectonics in the Northern Appalachians. *The Journal of Geology*, **104**, 185–195, https://doi.org/10.1086/629813

Viete, D.R. and Lister, G.S. 2017. On the significance of short-duration regional metamorphism. *Journal of the Geological Society, London*, **174**, 377–392, https://doi.org/10.1144/jgs2016-060

Wang, Y., Zhai, M. *et al*. 2021. Incipient charnockite formation in the Trivandrum Block, southern India: Evidence from melt-related reaction textures and phase equilibria modelling. *Lithos*, **380**, 105825, https://doi.org/10.1016/j.lithos.2020.105825

White, R.W., Powell, R., Holland, T.J.B., Johnson, T. and Green, E.C.R. 2014*a*. New mineral activity–composition relations for thermodynamic calculations in metapelitic systems. *Journal of Metamorphic Geology*, **32**, 261–286, https://doi.org/10.1111/jmg.12071

White, R.W., Powell, R. and Johnson, T. 2014*b*. The effect of Mn on mineral stability in metapelites revisited: new *a*–*x* relations for manganese-bearing minerals. *Journal of Metamorphic Geology*, **32**, 809–828, https://doi.org/10.1111/jmg.12095

Whitehouse, M.J. 2003. Rare earth elements in zircon: a review of applications and case studies from the Outer Hebridean Lewisian Complex, NW Scotland. *Geological Society, London, Special Publications*, **220**, 49–64, https://doi.org/10.1144/GSL.SP.2003.220.01.03

Xu, Z., Wang, Q. *et al*. 2015. Kinematics of the Tengchong Terrane in SE Tibet from the late Eocene to early Miocene: Insights from coeval mid-crustal detachments and strike-slip shear zones. *Tectonophysics*, **665**, 127–148, https://doi.org/10.1016/j.tecto.2015.09.033